

Ferromagnetism in LaFeO₃/LaNiO₃ Superlattices with High Curie Temperature

Tianlin Zhou^{1,2}, Fei Gao¹, Qinghua Zhang^{1,2}, Yuansha Chen^{1,2}, Xinzhe Hu¹, Yuzhou He¹, Yuchen Zhao^{1,2}, Jianjie Li^{1,2}, Minghang Li^{1,2}, Shaojin Qi^{1,2}, Fengxia Hu^{1,2}, Jirong Sun^{1,2}, Yunzhong Chen^{1,2*}, and Baogen Shen¹⁻⁴

¹Beijing National Laboratory of Condensed Matter Physics and Institute of Physics, Chinese Academy of Sciences, Beijing 100190, China

²School of Physical Sciences, University of Chinese Academy of Sciences, Beijing 100049, China

³Ganjiang Innovation Academy, Chinese Academy of Sciences, Ganzhou, Jiangxi 341000, China

⁴CAS Key Laboratory of Magnetic Materials and Devices and Zhejiang Province Key Laboratory of Magnetic Materials and Application Technology, Ningbo Institute of Materials Technology and Engineering, Chinese Academy of Sciences, Ningbo 315201, China

Email: yzchen@iphy.ac.cn

Interfacing complex oxides in atomically engineered layered structures can give rise to a wealth of exceptional electronic and magnetic properties that surpass those of the individual building blocks. Herein, we demonstrate a ferromagnetic spin order with a high Curie temperature of 608 K in superlattices consisting of otherwise paramagnetic perovskite LaNiO₃ (LNO) and antiferromagnetic LaFeO₃ (LFO). The extraordinary ferromagnetism likely results from the covalent exchange due to interfacial charge transfer from Fe to Ni cations. By deliberately controlling the thickness of the LNO sublayers thus the amount of charge transfer, a robust ferromagnetism of 4 μ_B is realized for a stacking periodicity consisting of one single unit cell of both LNO and LFO, an emergent double perovskite phase of La₂FeNiO₆ with B-site layered ordering configurations. The ferromagnetic

LFO/LNO superlattices offer great potential for the search of emergent magnetodielectric and/or multiferroic properties as well as applications in spintronics and electrocatalysts.

Introduction

Atomically engineered heterostructures of strongly correlated oxides have enabled the rational design of emergent interfacial magnetic and electric properties not present in the constituting layer [1-3]. The most prominent examples are the two-dimensional (2D) electron gas formed at the interface between two band-gap insulators [4,5], superconducting interfaces between non-superconducting cuprates [6], and the ferromagnetism between two antiferromagnetic materials [7]. Among the magnetically ordered materials, including ferromagnetic (FM), ferrimagnetic, and antiferromagnetic (AFM), FM and ferrimagnetic materials have significant technological importance in diverse applications, such as permanent magnets, microwave devices, sensors, magnetic recording and memory media [8]. Magnetic interfaces particularly those based on perovskite oxides, ABO_3 , are of similar technological importance, but the interface-induced changes to electronic structure, orbital occupancy, and charge redistribution in addition to metal-oxygen band hybridization often led to magnetic exchange interactions across B-O-B bonds different from those of the bulk [9-11]. Notably, although the charge transfer and the emerging functionalities at oxide heterointerfaces have been intensively investigated for early transition metal oxides [9, 11-14], the charge transfer across heterostructures consisting of two late transitional metal oxides remains less investigated [10, 15-17]. The research is even extremely rare when the thickness of the component for the heterointerface or the superlattice is precisely controlled down to a single unit cell (uc) of the perovskite oxide (approximately 0.4 nm) [18,19].

Rare-earth nickelate $RNiO_3$ (with R =rare-earth) is a typical family of late transition metal oxides, which have attracted significant interest in recent years due to their remarkable properties including sharp metal-to-insulator transitions (MIT) tunable with the R radius [19-21] as well as the emergency of superconductivity in the

infinitely layered $\text{Nd}_{0.8}\text{Sr}_{0.2}\text{NiO}_2$ thin films [22]. LaNiO_3 (LNO) is the only member of the rare earth perovskite $R\text{NiO}_3$ that is a Pauli paramagnetic (PM) metal with no signature of MIT or magnetic order at any temperature. Electronically, LNO is a charge transfer metal with strong hybridization between Ni $3d$ and oxygen $2p$ states, where the electronic configuration can be described as a superposition form $|\psi\rangle = \alpha|3d^7\rangle + \beta|3d^8\underline{L}\rangle$ (\underline{L} denotes a ligand hole on the oxygen ion) [23]. The system shows partial covalence, and the degree of covalence is given by the ratio between β^2 and α^2 ($\alpha^2 + \beta^2 = 1$). The hybridization between the $3d$ band and the oxygen $2p$ band results in the formation of oxygen holes and a small or negative charge transfer gap [21], which are key features of high-temperature superconducting cuprates [24]. Therefore, strain-engineered thin films or multilayers based on nickelates have been intensively investigated to explore electronic structures that would mimic those of cuprate parent materials [25], which prefer AFM order. Moreover, the low-lying Ni $3d$ bands of LNO with partial filling make it prone to electron acceptors. Notably, ferromagnetic-like behavior has been reported in the paramagnetic LNO layer when it is interfaced with another ferromagnetic layer of LaMnO_3 thin films [15,16] or a ferrimagnetic layer of GdTlO_3 [11]. But most of such charge-transfer-induced ferromagnetism shows Curie temperature below room temperature. In this Letter, we report a charge transfer induced ferromagnetism in the heterostructure of $\text{LaFeO}_3/\text{LaNiO}_3$ (LFO/LNO) (Fig.1a), where LFO is a G-type AFM insulator (Fig.1b) as electron donor, the amount of the transferred charge is controlled by the thickness of LNO on the scale of 1 uc. In the extreme limit of the single superlattice (SL) stacking periodicity (periodic lattice, p.l.) consisting of one unit cell (uc) pseudo-cubic LNO and one unit cell pseudo-cubic LFO, similar to the theoretically predicted double perovskite (DP) $\text{La}_2\text{NiFeO}_6$ [26], the SL shows not only a high magnetization of $4 \mu_B/\text{p.l.}$, but also a high Curie temperature of 608 K. The emergent properties are not observed either in the constituting materials (LFO and LNO) or the mixed compound $\text{LaFe}_{0.5}\text{Ni}_{0.5}\text{O}_3$ [27], which could result from the formation of an emergent DP phase of $\text{La}_2\text{FeNiO}_6$ with B -site layered ordering configurations along the (001)

orientation. The ability to affect interfacial charge transfer and the Ni 3d-O 2p covalency thus the Ni 3d-O 2p-Fe 3d exchange interactions through a precisely controlled approach, not realizable by conventional processing techniques, suggests a new avenue to realizing extraordinary FM materials.

Results

Creation of LNO_n/LFO₁ superlattices with layered ordering of cations

We have grown LNO_n/LFO_m superlattices (SLs) by alternately stacking LNO and LFO layers using pulsed laser deposition on SrTiO₃ (STO) (001) substrates (see Methods), where n and m represent the layer thickness of LNO and LFO in pseudo-cubic uc, respectively. Here n was varied from $n = 1$ to 5 uc, while the LFO layer was set to 1 uc thick. The LNO_n/LFO₁ bilayer was repeated 10-20 times to form the SL. The SL growth was monitored *in-situ* by reflection high-energy electron diffraction (RHEED). Streaked RHEED patterns with clear intensity oscillations were observed during the growth of both LNO and LFO films, implying a 2D layer-by-layer film growth mode (Supplementary Figure S1). The epitaxial growth of the high quality LNO_n/LFO₁ SLs was also confirmed by X-ray diffraction experiments and high-resolution scanning transmission electron microscopy (STEM). Notably, although clear Laue fringes are visible for all the SLs from high-resolution XRD θ - 2θ scans (Supplementary Figure S2) due to their atomically smooth surfaces as confirmed by atomic force microscopy (Supplementary Figure S3), the satellite peaks indicating the chemically modulated structure with well-defined interfaces were only visible for $n \geq 3$, consistent with the previous results on similar structure [17]. Moreover, for $n \leq 3$, the SL is under compressive strain with $c \geq 3.905$ Å. While as $n > 3$, the SL is under tensile strain. Such decrease of out of plane c with increasing n is consistent with the smaller lattice constant of LNO compared to LFO (LFO is orthorhombic with a pseudo-cubic lattice constant $a_0 = 3.93$ Å [17], and LNO is rhombohedral with pseudo-cubic $a_0 = 3.838$ Å). Figs. 1c and d show the atomically resolved high-angle annular dark-field (HAADF) image of the cross-section of the LNO₁/LFO₁ SL and

LNO₄/LFO₁ SL samples, respectively, recorded along the [100] zone axis. As the intensity of HAADF-STEM images is sensitive to atomic number (Z), both SLs show coherent epitaxial lattice as demonstrated by the brightest sublattice of the La ions. No dislocations, defects or any nano-scale phase-separated microstructures such as Fe or Ni metal clusters were observed. The compositional electron energy-loss spectroscopy (EELS) maps obtained from the analysis of the La $M_{4,5}$ (Fig.1e left), Fe $L_{2,3}$ (Fig.1e right), and Ni $L_{2,3}$ signals reveal the epitaxial growth of the periodic layered structure, which is flat and continuous over long lateral distances. Cation intermixing of Fe and Ni ions when occurs is found to be confined within 1-2 uc of LFO (within 1 p.l. of the SL). Shortly, high quality LNO _{n} /LFO₁ superlattices with layered ordering of configurations for Fe and Ni cations are successfully fabricated.

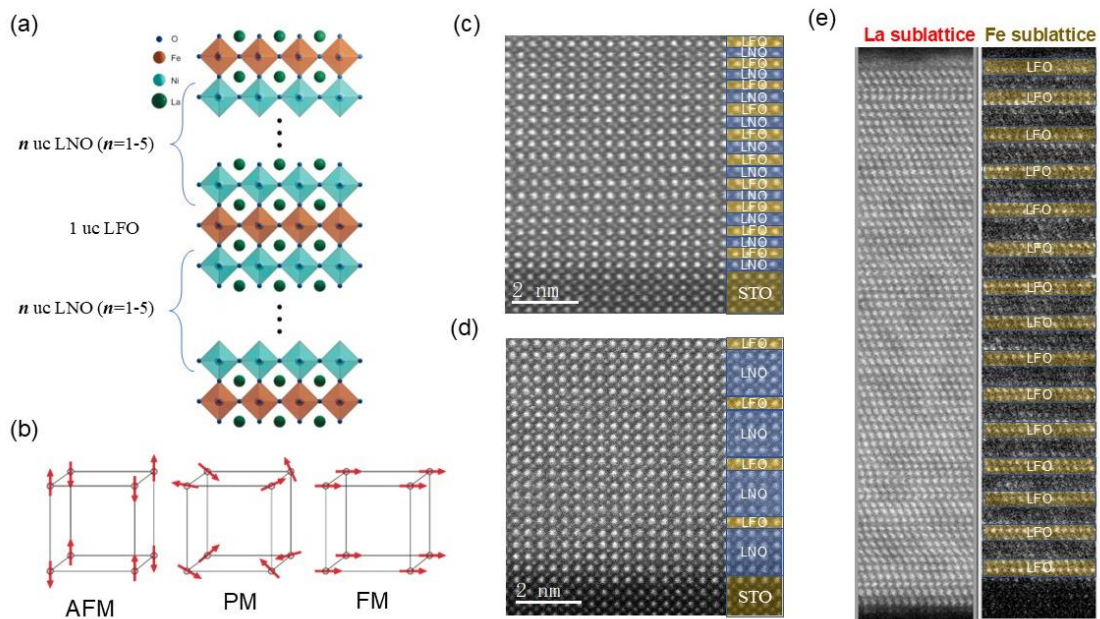


Fig.1 Epitaxial growth of the LNO _{n} /LFO₁ SLs. **a**, the sketch of the SL structure where the thickness of paramagnetic LNO, n , was varied from $n = 1$ to 5 uc, while the G-AFM LFO layer was set to 1 uc; **b**, the illustration for magnetic structures of G-AFM, paramagnetic (PM) and FM coupling; **c** and **d**, the cross-sectional STEM HAADF images of the LNO₁/LFO₁ and LNO₄/LFO₁ SL, respectively, recorded along the [100] zone axis. **e**, The EELS maps obtained from the analysis of the La $M_{4,5}$ (left)

and Fe L_{2,3} (right) signals reveal the epitaxial growth of the periodic structure and cation intermixing confined within 1-2 uc of LFO (within 1 p.l. of the SL).

Magnetic and transport properties of the emergent ferromagnetic superlattices

LNO is a paramagnetic metal, and LFO is a G-type AFM insulator with intralayer antiparallel spin alignments, which shows one of the highest ordering temperatures of perovskite oxide ($T_N \approx 740$ K). Remarkably, when they were epitaxially grown along the (001) directions but absent for the (110) and (111) directions (Supplementary Figure S4), the LNO_n/LFO₁ SLs show strong signatures of ferromagnetism, which depends critically on the stacking thickness, n , of LNO. Fig.2a shows the hysteresis curves of the LNO_n/LFO₁ SLs measured at 300 K, *i.e.* the dependence of the magnetization (M) as a function of the magnetic field B , which is saturated under the applied field above 3.5 kOe. All samples exhibited key characteristics of FM behavior, including hysteresis and remnant magnetization. At $n=5$, the SL shows weak saturation ferromagnetism similar to LaFe_{0.5}Ni_{0.5}O₃ thin films. Remarkably, as n decreases, the highest saturation magnetization increases significantly, reaching 252.8 emu/cm³ for $n=1$, approximately 4.0 μ_B /p.l., comparable to the 4.96 μ_B /f.u. (f.u.= formula unit) for the FM DP La₂NiMnO₆ [28], and much larger than that of the LaFe_{0.5}Ni_{0.5}O₃ thin films (Fig.2b). Fig.2c shows the temperature dependence of magnetization (M - T curve) for the typical LNO_n/LFO₁ ($n=1, 3$ and 5) SL samples in addition to the LaNi_{0.5}Fe_{0.5}O₃ film. The Curie temperature, T_C , could be determined based on the minimum value of the temperature coefficient TCM, defined as $TCM = 1/M(dM/dT)$. Remarkably, all the SL samples show a T_C much higher than room temperature, around $T_C=608$ K, 589 K and 419 K, respectively, for $n=1, 3$ and 5. It is also noteworthy that the LaNi_{0.5}Fe_{0.5}O₃ film shows a $T_C=109$ K, much lower than those of the SL but higher than the bulk spin glassy temperature of 83 K [27]. The results strongly suggest that a unique FM order is accessed in the SLs structures with the strongest magnetism obtained at $n=1$, an emergent La₂NiFeO₆ DP structure with B -site layered ordering configuration along (001) direction. As illustrated in Table 1, its T_C is close to the highest value ($T_C = 625$

K) reported for $\text{Sr}_2\text{CrReO}_6$ among the DP compounds [29]. The temperature dependent resistivity, ρ , of the $\text{LNO}_n/\text{LFO}_1$ ($n=1, 3$ and 5) SL sample was also measured between 2-300 K, as shown in Fig.2d. All the SLs show a semiconductive behavior with small polaron conduction mechanism ($n \leq 4$) (Supplementary Figure S5), although the $\text{LaFe}_{0.5}\text{Ni}_{0.5}\text{O}_3$ thin film is found to be highly insulating. This strong conduction difference, in addition to the strong difference in magnetism, may be related to the difference in the ordered arrangement of the Fe and Ni cation atoms over the B -sites, where the higher level of cations ordering prefers higher magnetization and higher conductivity [19]. We thus obtained an emergent $\text{La}_2\text{NiFeO}_6$ DP with Curie temperature much higher than room temperature, which has been predicted to be a half-metallic ferromagnet [26].

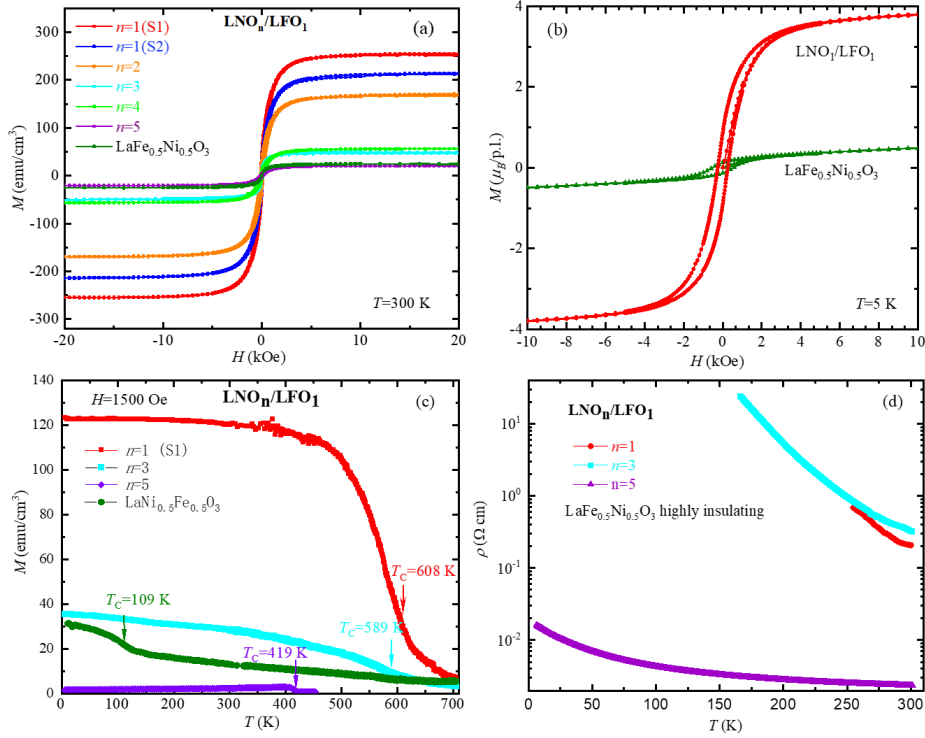


Fig.2 Magnetic and transport properties of the atomically engineered $\text{LNO}_n/\text{LFO}_1$ SLs. **a**, the hysteresis curves of the $\text{LNO}_n/\text{LFO}_1$ SLs measured at 300 K, for comparison the results of $\text{LaFe}_{0.5}\text{Ni}_{0.5}\text{O}_3$ thin films are also presented; **b**, the hysteresis curve of the $\text{LNO}_1/\text{LFO}_1$ SL measured at 5 K in comparison to the $\text{LaFe}_{0.5}\text{Ni}_{0.5}\text{O}_3$ thin film; **c**, the temperature dependence of magnetization for the $\text{LNO}_n/\text{LFO}_1$ ($n=1, 3$ and 5) SLs and the $\text{LaNi}_{0.5}\text{Fe}_{0.5}\text{O}_3$ film, measured at $H=1500$ Oe; **d**, the temperature dependent

resistivity, ρ , of the $\text{LNO}_n/\text{LFO}_1$ ($n=1, 3$ and 5) SLs, showing semiconductive behavior.

Table 1 | The emerging ferromagnetic SLs and the typical double perovskites (DP) with ferromagnetism near and above room temperature

Formula	Structure	Saturation magnetization	Curie Temperature
		M_s ($\mu_B/\text{p.l.}$ or f.u.)	T_C (K)
$\text{LaFeO}_3/\text{LaCrO}_3$ [7]	1:1 SL	3.0	375
$\text{LaNiO}_3/\text{LaMnO}_3$ [16]	7:7 SL	3.7.	175
$\text{LaNiO}_3/\text{LaFeO}_3$	1:1 SL	4.0	608
$\text{LaNiO}_3/\text{LaFeO}_3$	3:1 SL	1.3	589
$\text{La}_2\text{NiMnO}_6$ [28]	DP	4.96	280
$\text{Sr}_2\text{FeMoO}_6$ [29]	DP	3.98	345
$\text{Sr}_2\text{CrReO}_6$ [29]	DP	2.6	625

Magnetic domain microstructure characterized by magnetic force microscopy

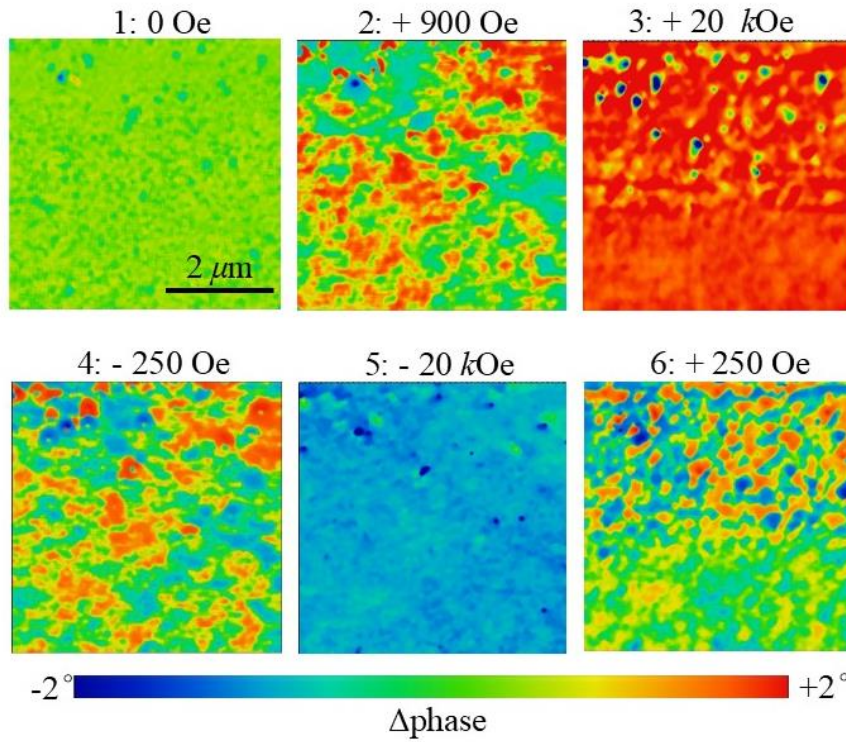


Fig.3 Magnetic force microscopy (MFM) domains structure of the $\text{LNO}_1/\text{LFO}_1$

SL sample obtained at 2 K. The magnetic contrasts ($\Delta\phi$) are represented by colors: the red (blue) colored area with positive (negative) $\Delta\phi$ represents the net magnetization projecting along the upward (downward) z direction, and the green colored area with nearly zero $\Delta\phi$ represents for domain walls or the grains with zero-magnetization.

The magnetic domain microstructure and its evolution with respect to the applied field for the LNO₁/LFO₁ SL were also investigated by magnetic force microscopy (MFM). Generally, the magnetograms obtained by MFM provide information of the effective magnetization along the z direction of the local domains. Fig.3 shows the magnetograms obtained at 2 K in different out-of-plane magnetic fields corresponding to the critical points on the M - H loop in Fig.2b. Here the red or blue-colored regions represent net-magnetization oriented up ($+M_z$) or down ($-M_z$), respectively, and the green color represents the zero M_z signal. As shown in Fig.3, the as-grown LNO₁/LFO₁ SL first demonstrates nearly zero-magnetization along the z direction after the zero-field-cooling (ZFC) process. By applying a positive magnetic field along the out-of-plane direction, discrete upward domains begin to appear and grow continuously (+ 900 Oe), eventually reaching an upward single-domain state at the saturation field of +20 kOe. By applying a negative magnetic field, the single-domain state turns to fragments of upward and downward domains at the coercive field of approximately -250 Oe, corresponding to the zero net magnetization in the M - H loop. The typical size of the fragment domains after magnetization (measured at +250 Oe) is about 300~500 nm (Supplementary Figure S6). The magnetic domain evolution is repeatable during the field sweeping process, as further evidenced by the downward single-domain state at -20 kOe and then the fragment-domain state at +250 Oe (the positive coercive field). The domain structures after ZFC and their evolution upon applying magnetic fields are consistent with the direct magnetization measurements. This further confirms that the strong magnetism is intrinsic to our SL samples, where the plausible magnetic contribution from the STO bulk substrate is negligible.

Discussion

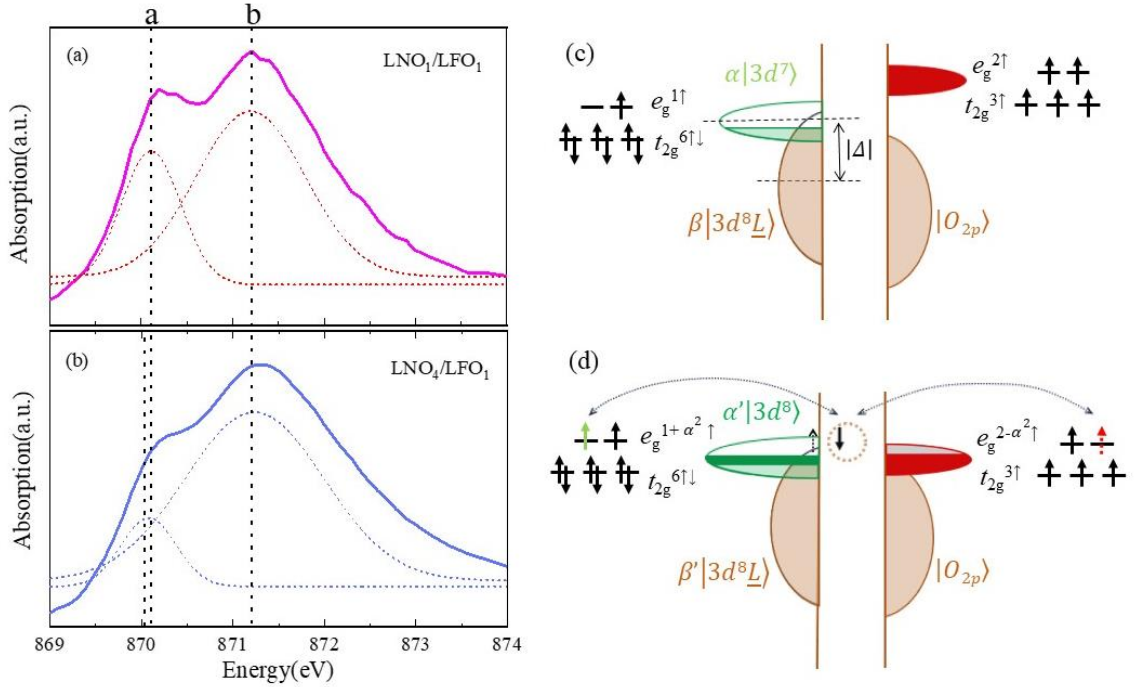


Fig.4 Charge transfer at the LNO_n/LFO₁ SL and a schematic representation of the covalent ferromagnetism in the LNO₁/LFO₁ SL. (a) and (b) The XAS signal of LNO₁/LFO₁ and LNO₄/LFO₁ near the Ni L₂ edge, respectively. All curves were fitted with two Gaussian functions, labeled as “a” and “b”. The fitting data were shown as thin dashed lines. (c) and (d) the schematic representation of the charge state before and after the charge transfer induced rehybridization process, respectively, from LFO to LNO.

The magnetic exchange interactions in 3d perovskite oxides occur through *d* orbitals (dominated mainly by e_g orbitals) centered at neighboring *B* cations bridged by an oxide ion, referred to as “super-exchange interaction”. The guidelines dubbed as the Goodenough-Kanamori-Anderson rules can be used to predict the ferromagnetic and antiferromagnetic states for transition-metal oxides [30]. The nominal Fe³⁺ ion in LFO has a $3d^5$ ($t_{2g}^{3\uparrow} e_g^{2\uparrow}$) configuration. It is AFM in accordance with the Goodenough-

Kanamori rules. The nominal Ni^{3+} ion has a $3d^7 (t_{2g}^6 e_g^1)$ configuration with filled t_{2g} orbitals and one electron residing in the doubly degenerate e_g orbitals. Due to the electron-acceptor nature of LNO as illustrated in Fig.4c, the strong ferromagnetism could originate from the electron transfer from the LFO to the LNO layer, which fills not only $\alpha|3d^7\rangle$ but also $\beta|3d^8L\rangle$ states, where the ferromagnetism at the interface could emerge from the covalent exchange coupling between Ni^{2+} and Fe^{4+} ions through the hybridization between the oxygen $2p$ band and the $3d$ band [31].

To determine the cation valence ($\text{Fe}^{3+}/\text{Fe}^{4+}$, $\text{Ni}^{3+}/\text{Ni}^{2+}$) thus the charge transfer in addition to their spatial distribution of the Fe-Ni system [32], X-ray absorption spectroscopy (XAS) measurements were performed on our $\text{LNO}_n/\text{LFO}_1$ ($n=1$ and 4) SL samples. The signal of the Fe $L_{2,3}$ edge was found to show roughly similar features between $\text{LNO}_1/\text{LFO}_1$ and $\text{LNO}_4/\text{LFO}_1$ samples, except that the splitting between the two Fe L_3 peaks of the $\text{LNO}_1/\text{LFO}_1$ was slightly wider than that of the $\text{LNO}_4/\text{LFO}_1$ sample (Supplementary Figure S7). In contrast, the XAS signal at the Ni $L_{2,3}$ edge, after correction for the overlap of the La $M_{4,5}$ signal, shows a distinct difference between $\text{LNO}_1/\text{LFO}_1$ and $\text{LNO}_4/\text{LFO}_1$ (Supplementary Figure S7). The shape of the spectra in our SL samples clearly deviates from that of the LNO film [33], which readily indicates a different formal Ni oxidation state. Particularly, as shown in Figs. 4a and b, we compared the Ni L_2 -edge region for the $\text{LNO}_1/\text{LFO}_1$ and $\text{LNO}_4/\text{LFO}_1$ samples. This region has no overlap with La edges and shows quite distinct features between Ni^{3+} and Ni^{2+} thus can gain insight into the Ni valence in our samples as reported previously [11]. The Ni L_2 experimental spectra for the $\text{LNO}_1/\text{LFO}_1$ and $\text{LNO}_4/\text{LFO}_1$ samples were fitted with two Gaussian peaks labeled as ‘a’ and ‘b’. The changes in the spectral shape, particularly the sharpening of the low-energy feature (labeled ‘a’), are reminiscent of the signature of Ni^{2+} in the NiO [34]. By comparing the relative intensity of the two features (‘a’ and ‘b’), it is clear that the Ni valence is stronger reduced towards $2+$ for the $\text{LNO}_1/\text{LFO}_1$ sample than the $\text{LNO}_4/\text{LFO}_1$ sample. These results not only confirm the charge transfer from Fe to Ni ions in the $\text{LNO}_n/\text{LFO}_1$ SL samples, but also reveal a

strong dependence of the amount of transferred electrons on the thickness of the nickelate, where the charge transfer length is in a short range nature and strongly confined to the proximity of the interface.

Upon charge transfer, the filling of the $\text{Ni}^{3+} \alpha|3d^7\rangle$ will increase towards $\text{Ni}^{2+} \alpha'|3d^8\rangle$ and the level of the corresponding subband will decrease, thus the overlapping or the hybridization between the $3d$ band and the oxygen $2p$ band $\beta'|3d^8\underline{L}\rangle$ will also increase, as illustrated in Fig.4d. This rehybridization process requires a redistribution of electrons between the $|3d^7\rangle$ and the $|3d^8\underline{L}\rangle$ states, which occurs at an energy cost $|\Delta|$ for each electron transferred between $|3d^8\underline{L}\rangle$ and $\alpha|3d^7\rangle$, but thanks to the presence of $\alpha'|3d^8\rangle$, the $|\Delta|$ is expected to be decreased after charge transfer and the rehybridization is more prone to occur. On the other hand, due to the strong covalent character of LNO with a large rare-earth size, which increases the cost of rehybridization, the competition between the charge transfer, controlled by the energy gain associated with the difference in electron affinity, and the cost of rehybridization, limits the amount of electrons that can be transferred across the interface. Notably, changes in the multiplet splitting of the Ni L_3 absorption edge can be used to estimate the level of covalence [35]. This splitting corresponds to the energy separation between t_{2g} and e_g levels resulting from the interplay between hybridization and Coulomb repulsion, which are both stronger for e_g levels. Previous studies have shown that the larger splitting of the L_3 peaks indicates a decrease in covalence [11,34]. The fitted XAS at the Ni L_3 edge also indicates that peak splitting increases from $\text{LNO}_1/\text{LFO}_1$ to the $\text{LNO}_4/\text{LFO}_1$ samples, reflecting a decrease in covalence, where a weakened ferromagnetism is also observed. These results suggest that the charge transfer from Fe^{3+} to Ni^{3+} indeed results in an increase of covalence, favoring the ferromagnetic Ni^{2+} - O^{2-} - Fe^{4+} interactions [31]. The hybridization and charge transfer along the interfacial Fe-O-Ni bonds are mainly proposed to explain the ferromagnetism across the interface and on the Ni site. As for the magnetic nature of the LFO single layer, in contrast to the bulk G-AFM configuration, it probably exhibits a helicoidal magnetic (HM) ordering

due to the negative charge transfer energy and the enhanced oxygen-oxygen hopping amplitude when it is interfaced with LNO upon charge transfer [36]. It is noteworthy that X-ray magnetic circular dichroism (XMCD) measurements showed negligible local Fe or Ni moments at the Fe $L_{2,3}$ and Ni $L_{2,3}$, although they were found to be coupled ferromagnetically to each other. As for the fact that the estimated Fe and Ni moment from XMCD is significantly lower than that measured by the SQUID magnetometry, it might result from the presence of a surface layer with a strongly reduced FM signal as the XMCD measurement was performed in total electron yield configuration, which is very surface sensitive and probes only a few nano-meter deep. Similar huge deviations have been also observed in BaFeO_3 thin films [37] and for $\text{LaMnO}_3/\text{LaNiO}_3$ superlattices [16]. Therefore, the exact origin of the strong ferromagnetism remains under investigation.

Conclusions

Shortly, robust ferromagnetism with high magnetization and Curie temperature much above room temperature was achieved in $\text{LNO}_n/\text{LFO}_1$ SL by precisely controlling the charge transfer as well as the interfacial orbital hybridization in late transitional metal oxides. The latter is viable for tuning the strength of the exchange interactions in all-oxide heterostructures. The semiconducting and FM $\text{LNO}_1/\text{LFO}_1$ SL, which can be regarded as an emergent DP phase of $\text{La}_2\text{FeNiO}_6$ with *B*-site layered ordering configurations along the (001) orientation, can have a wide spectrum of applications for spintronics.

Methods:

Sample fabrication and characterization:

High quality LNO_n/LFO₁ SLs were epitaxially grown on (001)-oriented STO substrates by pulsed laser deposition (KrF, $\lambda=248$ nm) with 10-20 repetitions. During film growth, the substrate temperature was kept at 620°C and the oxygen pressure was set to 3.4×10^{-2} mbar. The fluence of the laser pulse was 1.2 J/cm^2 , and the repetition rate was 2 Hz. The SL growth was monitored *in-situ* by reflection high-energy electron diffraction (RHEED). Layer by layer epitaxial growth was achieved for both the LNO and LFO layers. After deposition, the sample was cooled to room temperature under the oxygen pressure of 0.1 mbar. The crystal structure of the superlattice was observed by X-ray diffraction (XRD).

The magnetic properties were measured by a Quantum-Designed vibrating sample magnetometer (VSM-SQUID). The *M-T* measurements were performed in two temperature ranges from 2-300 K and 300 K-750 K using the same system with an oven option. The transport measurement was measured by a physical properties measurement system (PPMS) at temperatures from 5-300 K.

MFM measurements were performed in a variable temperature system from attocube equipped with a superconducting magnet (attoDRY2100). All measurements were conducted in vacuum at 2 K, based on a phase modulation technique in noncontact mode, with a cantilever (PPP-MFMR) with a spring constant $k \sim 2.8 \text{ N/m}$ and a resonant frequency $f \sim 75 \text{ kHz}$.

Scanning transmission electron microscopy (STEM): For cross-sectional microscopy, the sample was prepared by using focused ion beam (FIB) milling. Cross-sectional lamellas were thinned down to 60 nm thick at an accelerating voltage of 30 kV with a decreasing current from the maximum 2.5 nA, followed by fine polish at an accelerating voltage of 2 kV with a small current of 40 pA. STEM measurements were conducted by a double Cs-corrected JEOL JEM-ARM200CF operated at 200 kV with a CEOS Cs corrector (CEOS GmbH, Heidelberg, Germany).

X-ray absorption spectroscopy (XAS): Resonant X-ray reflectometry (RXR) experiments were carried out at the REIXS beamline of the Canadian Light Source at 300 K in an ultrahigh vacuum environment.

References:

- [1] Rijnders, G. & Blank, D. H. A. Build your own superlattice. *Nature* **433**, 369–370 (2005)
- [2] H. Y. Hwang, Y. Iwasa, M. Kawasaki, B. Keimer, N. Nagaosa & Y. Tokura, Emergent phenomena at oxide interfaces, *Nature Mater.* **11**, 103-113 (2012)
- [3] W. Reiner, F. J. Walker, C. H. Ahn, Atomically Engineered Oxide Interfaces, *Science* **323**, 1018 (2009)
- [4] A. Ohtomo & H. Y. Hwang, A high-mobility electron gas at the LaAlO₃/SrTiO₃ heterointerface, *Nature* **427**, 423–426 (2004)
- [5] Chen et al. A high-mobility two-dimensional electron gas at the spinel/perovskite interface of γ -Al₂O₃/SrTiO₃, *Nature Commun.* **4**, 1371 (2013)
- [6] A. Gozar, G. Logvenov, L. Fitting Kourkoutis, A. T. Bollinger, L. A. Giannuzzi, D. A. Muller & I. Bozovic, High-temperature interface superconductivity between metallic and insulating copper oxides, *Nature* **455**, 782-785 (2008)
- [7] Kenji Ueda, Hitoshi Tabata, Tomoji Kawai, Ferromagnetism in LaFeO₃-LaCrO₃ Superlattices, *Science* **280**, 1064 (1998)
- [8] J. M. D. Coey, Magnetism and Magnetic Materials, Cambridge University Press 617pp. (2018)
- [9] Frances Hellman *et al.* Interface-induced phenomena in magnetism, *Rev. Mod. Phys.* **89**, 025006 (2017)
- [10] Paul C. Rogge, Padraic Shafer, Gilberto Fabbris, Wen Hu, Elke Arenholz, Evguenia Karapetrova, Mark P. M. Dean, Robert J. Green, and Steven J. May, Depth-Resolved Modulation of Metal-Oxygen Hybridization and Orbital Polarization across Correlated Oxide Interfaces, *Adv. Mater.* **31**, 1902364 (2019)
- [11] M.N.Grisolia, J. Varignon, G. Sanchez-Santolino, A. Arora, S. Valencia, M. Varela, R. Abrudan, E. Weschke, E. Schierle, J. E. Rault, J.-P. Rue, A.Barthélemy, J. Santamaria, and M.Bibes, Hybridization-controlled charge transfer and induced magnetism at correlated oxide interfaces, *Nature Phys.* **12**, 484 (2016).
- [12] J. E. Kleibeuker, Z. Zhong, H. Nishikawa, J. Gabel, A. Müller, F. Pfaff, M. Sing, K. Held, R. Claessen, G. Koster, and G. Rijnders, Electronic Reconstruction at the Isopolar LaTiO₃/LaFeO₃ Interface: An X-Ray Photoemission and Density-Functional Theory Study, *Phys. Rev. Lett.* **113**, 237402 (2014)
- [13] Yanwei Cao, Xiaoran Liu, M. Kareev, D. Choudhury, S. Middey, D. Meyers, J.-W. Kim, P. J. Ryan, J.W. Freeland & J. Chakhalian, Engineered Mott ground state in a LaTiO_{3+ δ} /LaNiO₃ heterostructure, *Nature Commun.* **7**, 10418 (2016)
- [14] M.J. Han, Xin Wang, C.A. Marianetti, and A.J. Millis, Dynamical Mean-Field Theory of Nickelate Superlattices, *Phys. Rev. Lett.* **107**, 206804 (2011)
- [15] Marta Gibert, Pavlo Zubko, Raoul Scherwitzl, Jorge Íñiguez and Jean-Marc Triscone, Exchange bias in LaNiO₃-LaMnO₃ superlattices, *Nature Mater.* **11**, 195 (2012)
- [16] C. Piamonteze, M. Gibert, J. Heidler, J. Dreiser, S. Rusponi, H. Brune, J.-M. Triscone, F. Nolting, and U. Staub, Interfacial properties of LaMnO₃/LaNiO₃

- superlattices grown along (001) and (111) orientations, *Phys. Rev. B* **92**, 014426 (2015)
- [17] Binbin Chen, Nicolas Gauquelin, Daen Jannis, Daniel M. Cunha, Ufuk Halisdemir, Cinthia Piamonteze, Jin Hong Lee, Jamal Belhadi, Felix Eltes, Stefan Abel, Zoran Jovanović, Matjaž Spreitzer, Jean Fompeyrine, Johan Verbeeck, Manuel Bibes, Mark Huijben, Guus Rijnders, and Gertjan Koster, Strain-Engineered Metal-to-Insulator Transition and Orbital Polarization in Nickelate Superlattices Integrated on Silicon, *Adv. Mater.* **32**, 2004995 (2020)
- [18] J. P. Bange, V. Roddatis, L. Schüler, F. Lyzwa, M. Keunecke, S. Lopatin, V. Bruchmann-Bamberg, and V. Moshnyaga, Charge Transfer Control of Emergent Magnetism at SrMnO₃/LaMnO₃ Interfaces, *Adv. Mater. Interfaces* **9**, 2201282 (2022)
- [19] P. Ksoll, R. Mandal, C. Meyer, L. Schüler, V. Roddatis, and V. Moshnyaga, Emergent double perovskite phase at LaMnO₃/LaNiO₃ interfaces: Coupled charge transfer and structural reconstruction. *Phys. Rev. B* **103**, 195120 (2021)
- [20] Torrance, J. B., Lacorre, P., Nazzari, A.I., Ansaldo, E. J. & Niedermayer, C. Systematic study of insulator-metal transitions in perovskites RNiO₃ (R=Pr, Nd, Sm, Eu) due to closing of charge-transfer gap. *Phys. Rev. B* **45**, 8209–8212 (1992).
- [21] Valentina Bisogni, Sara Catalano, Robert J. Green, Marta Gibert, Raoul Scherwitzl, Yaobo Huang, Vladimir N. Strocov, Pavlo Zubko, Shadi Balandeh, Jean-Marc Triscone, G. Sawatzky & Thorsten Schmitt, Ground-state oxygen holes and the metal–insulator transition in the negative charge-transfer rare-earth nickelates, *Nature Commun.* **7**, 13017 (2016)
- [22] Danfeng Li, Kyuho Lee, Bai Yang Wang, Motoki Osada, Samuel Crossley, Hye Ryoung Lee, Yi Cui, Yasuyuki Hikita & Harold Y. Hwang, Superconductivity in an infinite-layer nickelate, *Nature* **572**, 624-627 (2019)
- [23] J. Zaanen, G. A. Sawatzky & J. W. Allen, Band gaps and electronic structure of transition-metal compounds. *Phys. Rev. Lett.* **55**, 418 (1985).
- [24] F. Zhang & T. Rice, Effective Hamiltonian for the superconducting Cu oxides. *Phys. Rev. B* **37**, 3759-3761 (1988)
- [25] A. Boris et al. Dimensionality Control of Electronic Phase Transitions in Nickel-Oxide Superlattices, *Science* **332**, 937 (2011).
- [26] Shuhui Lv, Hongping Li, Xiaojuan Liu, Deming Han, Zhijian Wu, and Jian Meng, A New Half-Metallic Ferromagnet La₂NiFeO₆: Predicted from First-Principles Calculations, *J. Phys. Chem. C* **114**, 16710-16715 (2010)
- [27] M. Gateshki, L. Suescun, S. Kolesnik, J. Mais, K. Swierczek, S. Short, B. Dabrowski, Structural, magnetic and electronic properties of LaNi_{0.5}Fe_{0.5}O₃ in the temperature range 5-1000 K, *Journal of Solid State Chemistry* **181**, 1833-1839 (2008)
- [28] N. S. Rogado, J. Li, A. W. Sleight, M. A. Subramanian. Magnetocapacitance and Magnetoresistance Near Room Temperature in a Ferromagnetic Semiconductor: La₂NiMnO₆, *Adv. Mater.* **17**, 2225 (2005)

- [29] D. Serrate, J. M. De Teresa, and M. R. Ibarra, Double perovskites with ferromagnetism above room temperature, *J. Phys.: Condens. Matter* **19** 023201 (2007)
- [30] J. B. Goodenough, Theory of the Role of Covalence in the Perovskite-Type Manganites (La M(II))MnO₃, *Phys. Rev.* **100**, 564 (1955)
- [31] J. B. Goodenough, Covalent Exchange vs Superexchange in Two Nickel Oxides, *J. Solid. State. Chem.* **127**, 126 (1996)
- [32] L. Wang *et al.* Understanding the Electronic Structure Evolution of Epitaxial LaNi_{1-x}Fe_xO₃ Thin Films for Water Oxidation, *Nano Lett.* **21**, 8324–8331 (2021)
- [33] E. Sakai *et al.* Gradual localization of Ni 3d states in LaNiO₃ ultrathin films induced by dimensional crossover. *Phys. Rev. B* **87**, 075132 (2013).
- [34] S. Middey *et al.* Polarity compensation in ultra-thin films of complex oxides: the case of a perovskite nickelate. *Sci. Rep.* **4**, 6819 (2014).
- [35] C. Piamonteze *et al.* Spin-orbit-induced mixed-spin ground state in RNiO₃ perovskites probed by x-ray absorption spectroscopy: insight into the metal-to-insulator transition. *Phys. Rev. B* **71**, 020406 (2005).
- [36] Maxim Mostovoy, Helicoidal Ordering in Iron Perovskites, *Phys. Rev. Lett.* **94**, 137205 (2005)
- [37] T. Tsuyama *et al.* X-ray spectroscopic study of BaFeO₃ thin films: An Fe⁴⁺ ferromagnetic insulator. *Phys. Rev. B* **91**, 115101 (2015)

Acknowledgements

The discussions with R. Green and C. Piamonteze are greatly appreciated. The authors thank the support from the Science Center of the National Science Foundation of China (52088101), the National Key Research and Development Program of China (2023YFA1406400, 2021YFA1400300), the National Natural Science Foundation of China (51327806, 52072400, 52322212, T2394472, T2394470), and the support from the Synergetic Extreme Condition User Facility (SECUF). Part or all of the research described in this paper was performed at the Canadian Light Source, a national research facility of the University of Saskatchewan, which is supported by the Canada Foundation for Innovation (CFI), the Natural Sciences and Engineering Research Council (NSERC), the Canadian Institutes of Health Research (CIHR), the Government of Saskatchewan, and the University of Saskatchewan.

Author contributions

Y.Z.C. designed the concept and experiments. T.L.Z, F.G, S.J.Q fabricated the samples

and performed magneto-transport characterization. Y.S.C performed the MFM experiment and data analysis. H.Y.Z, Q.H. Z performed the STEM measurements and analysis. All authors discussed the results, interpretations, and wrote the manuscript.

Competing interests: The authors declare that they have no competing interests.

Data and materials availability: All data needed to evaluate the conclusions in the paper are present in the paper and/or the Supplementary Materials. Additional data related to this paper may be requested from the authors.